Constructing Well-Defined and Robust Th-MOF-Supported Single-Site Copper for Production and Storage of Ammonia from Electroreduction of Nitrate

Zhi Gao, Yulian Lai, Yuan Tao, Longhui Xiao, Liuxin Zhang and Feng Luo*

State key Laboratory of Nuclear Resources and Environment, School of Biology, Chemistry and Material Science, East China University of Technology, Fuzhou, Jiangxi 344000, China. Email: ecitluofeng@163.com

Experimental Procedures

1.1. Synthesis of Th-BPYDC. A mixture of 2,2'-bipyridine-5,5'-dicarboxylic acid (BPYDC; 0.05 mmol , 12.21 mg), $Th(NO_3)_4$ (0.05 mmol, 24.00 mg), and ionic liquid of tetramethylguanidine chloride (0.05 mmol, 7.58 mg), nitric acid (150 μL) was added into 3 mL *N,N′*-dimethylformamide (DMF) in a screw-capped glass capped jar (10 mL), followed by heating at 120 ℃ for 72 h. After cooling down to room temperature, the resulting mixture was washed with DMF and colorless octahedral crystals were collected and dried in air.

1.2. Synthesis of Cu@Th-BPYDC. Firstly, 10 mg Th-BPYDC crystals was placed in a screw-capped glass capped jar (10 mL) containing 5 mL saturated $CuCl_2$ solution using acetonitrile as solvent. Then, the mixture was heated at 80 °C for 7 days, resulting in a color change of the crystals to green.

1.3. Material Characterization. Crystalline structure of Th-BPYDC and Cu@Th-BPYDC were collected at room temperature on a Bruker-AXS SMART

Breeze CCD diffractometer using graphite monochromated Cu Kα radiation (λ = 1.54178 Å). Powder X-ray diffraction (PXRD) analysis of all samples were taken on a Bruker AXSD8 Discover powder diffractometer with Cu Kα radiation (k = 0.154 nm). Low temperature N_2 isotherms were recorded at 77 K on Micromeritics ASAP2020 instrument using ultrahigh-purity-grade (>99.999%) N_2. Thermogravimetric analysis (TGA) was carried out over a TGA Q500 thermal analysis system under air atmosphere. The Cu content of Cu@Th-BPYDC was determined by Shimadzu ICPS-7500 inductively coupled plasma emission spectrometer (ICP-AES). Temperature programmed desorption of NH_3 (NH_3–TPD) measurements were carried out on the AutoChem II. 2920 instrument (Micromeritics, USA).

1.4. Electrochemical measurements. Electrochemical measurements were performed on a CHI 660D electrochemical workstation (Chenhua, Shanghai) using a typical H-type electrolytic cell separated by a membrane in a strand three-electrode system. The catalyst inks were prepared by adding 3 mg catalyst into 1 mL solution including 0.95 mL ethyl alcohol and 50 μL Nafion solution, followed by ultrasonication for 30 min. Finally, 50 μL of above ink was dripped on the carbon paper (1×1 cm^{-2}) and then dried at room temperature. Carbon electrode, saturated calomel electrode and the as-prepared catalyst were used as counter electrode, reference electrode and working electrode, respectively. Before nitrate electroreduction measurement, the cathode electrolyte was purged with Ar (99.99% purity) for 30 min. The linear sweep voltammetry (LSV) was conducted in at a scan rate of 5 mV s^{-1} to obtain the polarization curves. The potentiostatic test was

conducted at different potentials for 2 h. The electrochemically active surface area (ECSA) of different catalysts was determined based on the double-layer capacitance (C_{dl}) using a simple cyclic voltammetry method in a non-Faradic potential range of 1.023-1.123 V vs RHE. By plotting the capacitive density at 1.073 V vs RHE against the scan rate (10, 20, 40, 60, 80 and 100 mV s^{-1}), a linear trend was observed. The slope of the fitted line was the twice of C_{dl}. The current density normalized to the electrochemically active surface area (ECSA) was calculated according to the equation of $J_{ECSA} = I/S_{ECSA}$, where J_{ECSA} = current density normalized by ECSA; I = current density (mA); $S_{ECSA} = C_{dl}/C_s$ (C_{dl} = double layer capacitance, C_s = 29 μF cm^{-2}). Electrochemical impedance spectroscopy (EIS) measurements were carried out over a frequency range from 100 kHz to 0.1 Hz at the at the potential of 0 V vs RHE.

1.5. NH_3 detection. The concentration of NH_3 product was detected by a colorimetric method using Nessler's reagent. Owing to the large concentration of NH_3 products, the obtained reaction solutions were diluted to appropriate concentration to match the range of calibration curves.

1.6. Computational formula. The Faradaic efficiency of electroreduction of NO_3^- to NH_3 was calculated following the equation of Faradaic efficiency = $(8F \times c \times V)/(M \times Q)$, where F is the Faraday constant (96485 C/mol), c is the measured NH_3 concentration, V is the volume of the electrolyte, M is the relative molecular mass and Q is the total charge used for electrosynthesis. The amount of NH_3 produced at a specific time was calculated using the $n = (c \times V)$.

1.7. $^{15}NO_3^-$ isotopic labelling tracer experiment. $^{15}NO_3^-$ (99 atom%) with the

concentration of 100 mM was used as the feeding N-source to perform the isotopic labeling nitrate reduction experiments to clarify the source of ammonia.

1.8. NH_3 sorption measurements. Isotherm of NH_3 at 298 K was collected on Micromeritics ASAP2020 instrument. Prior to the NH_3 adsorption measurements, samples were activated by heating at 100 ˚C overnight under high vacuum.

1.9. Static NH_3 vapor sorption. Typically, the activated Cu@Th-BPYDC (20 mg) was placed in a small vial (1.5 mL). Then the vial packed Cu@Th-BPYDC was placed in a large wide-mouth bottle (100 mL) containing electrolyte after stability test. The large bottle was sealed and kept in a heated oven at 50 °C. After a certain contact time, the large bottle was taken out and cooled to room temperature. The weight of the small vial containing the Cu@Th-BPYDC sample was then measured. This procedure was terminated once the weight of the Cu@Th-BPYDC did not change. For comparison, the uptake ability of Cu@Th-BPYDC toward pure H_2O was also measured by the same procedure.

1.10. DFT theoretical calculation. The structures were optimized at the method of CAM-B3LYP[1-4] level of theory using Gaussian 16 program package,[5] where the metal element Cu was using the pseudopotential basis set exchange dgauss-a2-dftxfit,[6,7] the others were using the all electron basis set 6-311++G(d,p). For each stationary points, further frequency calculations were performed to ensure there were no imaginary frequencies at same method and basis set. The binding energy ΔE_{bind} for ligand adsorbing NH_3 was calculated by Eq. 1, and then, with the addition of metals Cu, the adsorption energy was calculated by Eq. 2,

$$\Delta E_{bind} = E_{ligand\text{-}NH_3} - E_{ligand} - E_{NH_3} \quad (1)$$

$$\Delta E_{bind} = E_{ligand-Cu-NH_3} - E_{ligand-Cu} - E_{NH_3} \quad (2)$$

where $E_{ligand\text{-}Cu\text{-}NH3}$ and $E_{ligand\text{-}NH3}$ are the total energy of adsorbed structures; E_{ligand} and $E_{ligand\text{-}Cu}$ are the total energies of single ligand; E_{NH3} is the energy of NH_3.

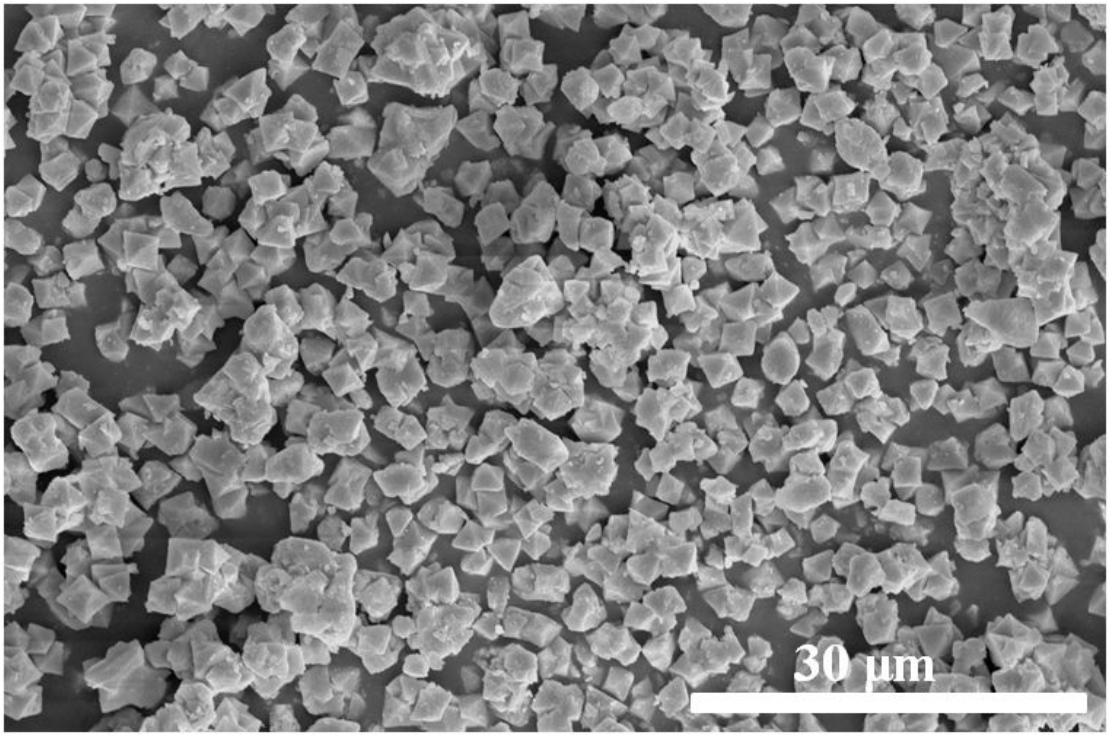

Figure S1. SEM image of Cu@Th-BPYDC.

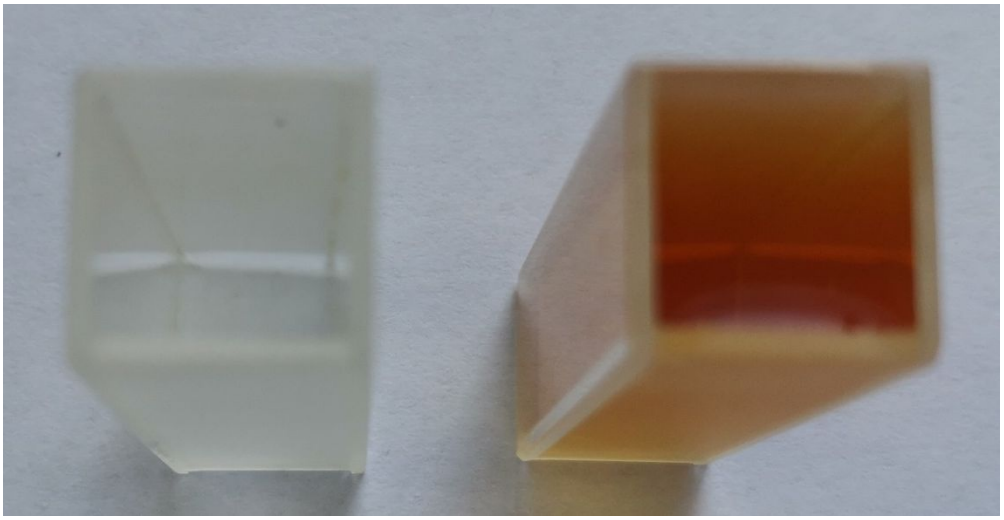

Figure S2. The chromogenic results of the electrolyte obtained after reaction without (left) and with (right) KNO_3 tested by Nessler's reagents.

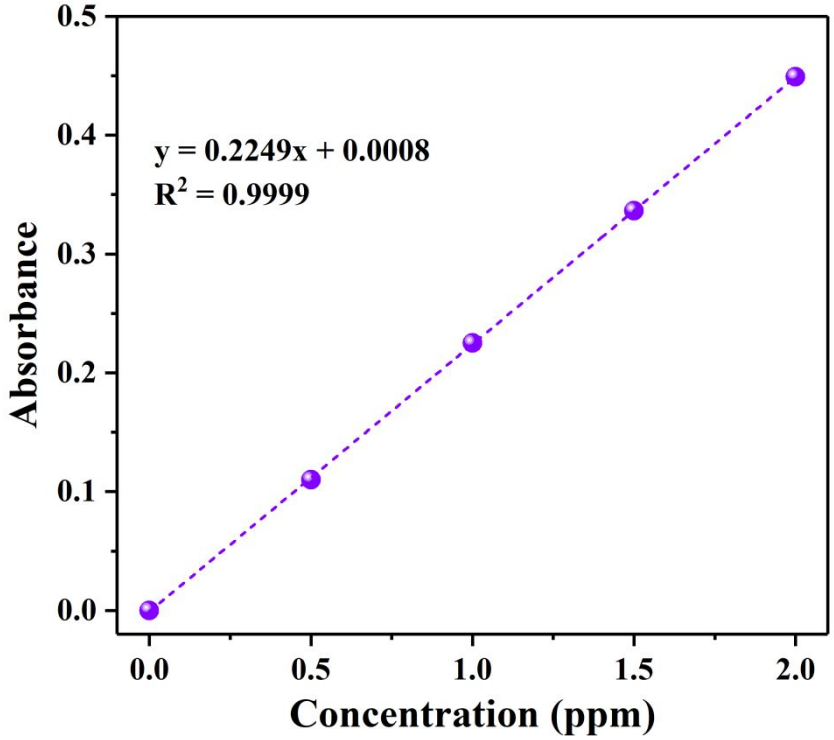

Figure S3. The linear standard curve for the calculation of NH_3 production.

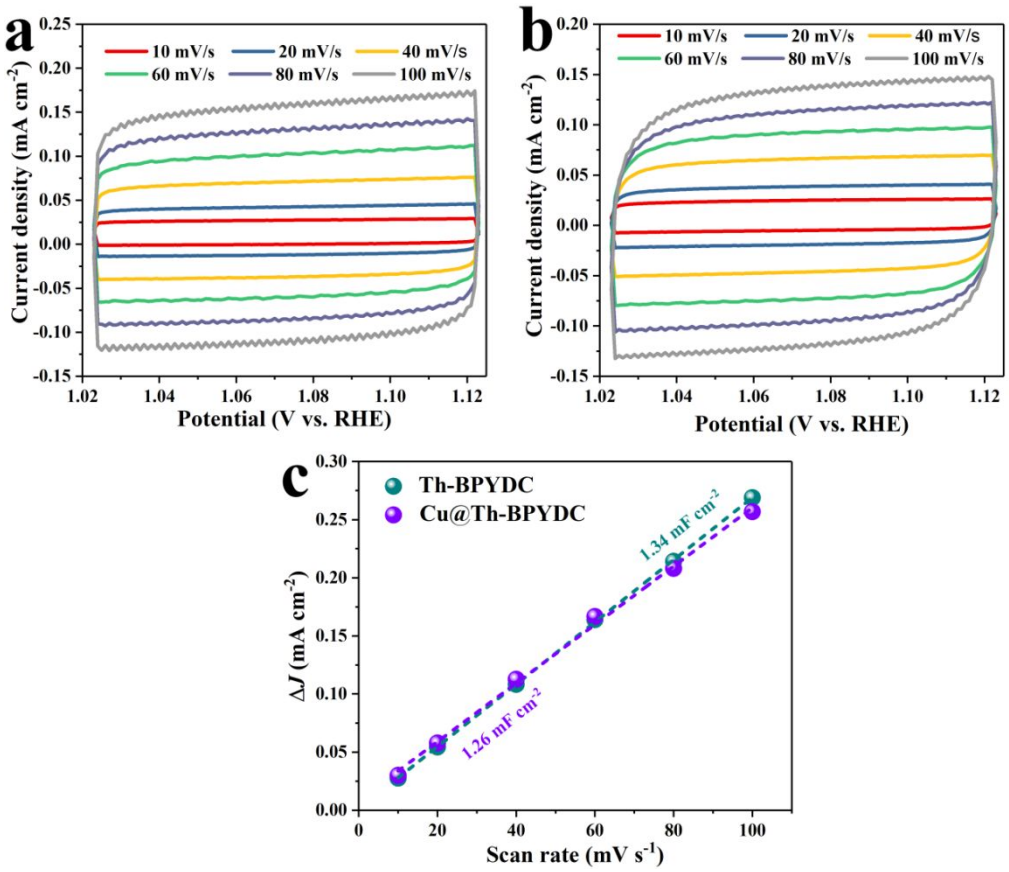

Figure S4. CV plots of Th-BPYDC (a) and Cu@Th-BPYDC (b) tested at various scan rates from 10 to 100 mV s^{-1}; ECSA evaluation (c).

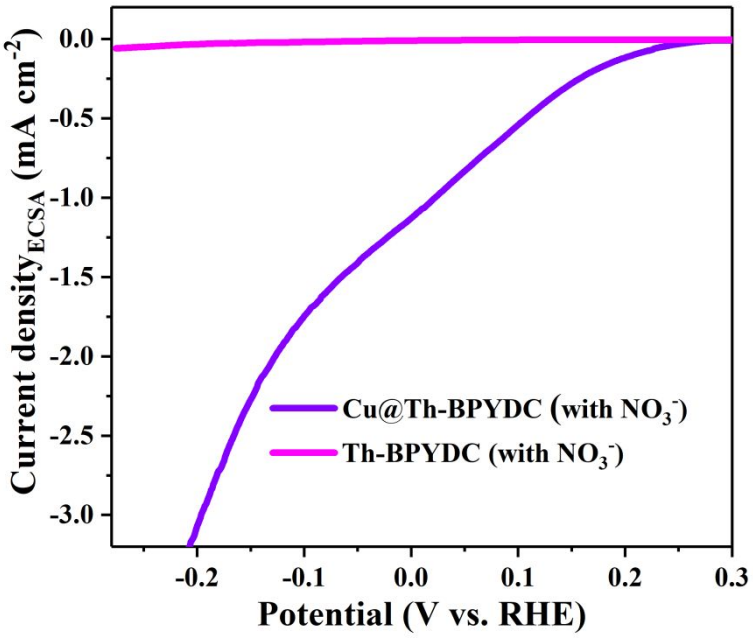

Figure S5. ECSA-normalized current densities.

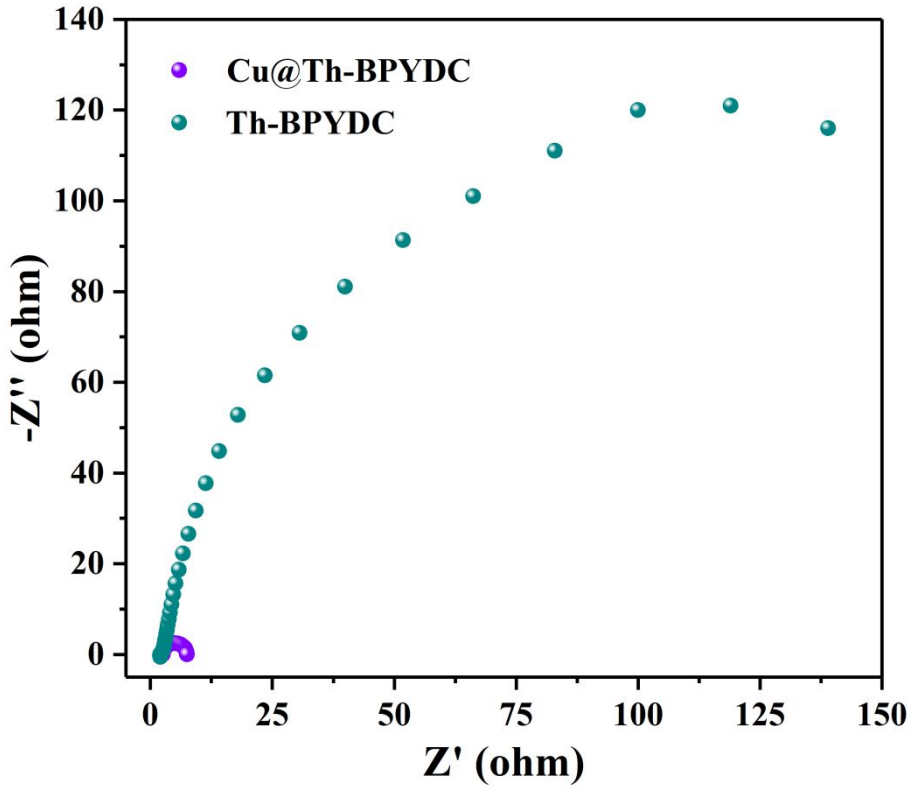

Figure S6. Nyquist plots measured at the potential of 0 V vs RHE.

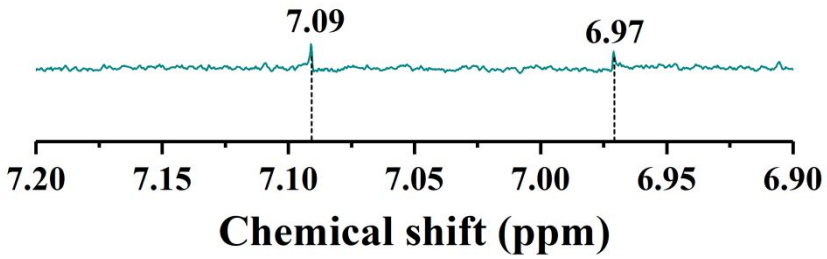

Figure S7. ^{1}H NMR spectrum using $^{15}NO_3^-$ as nitrogen source.

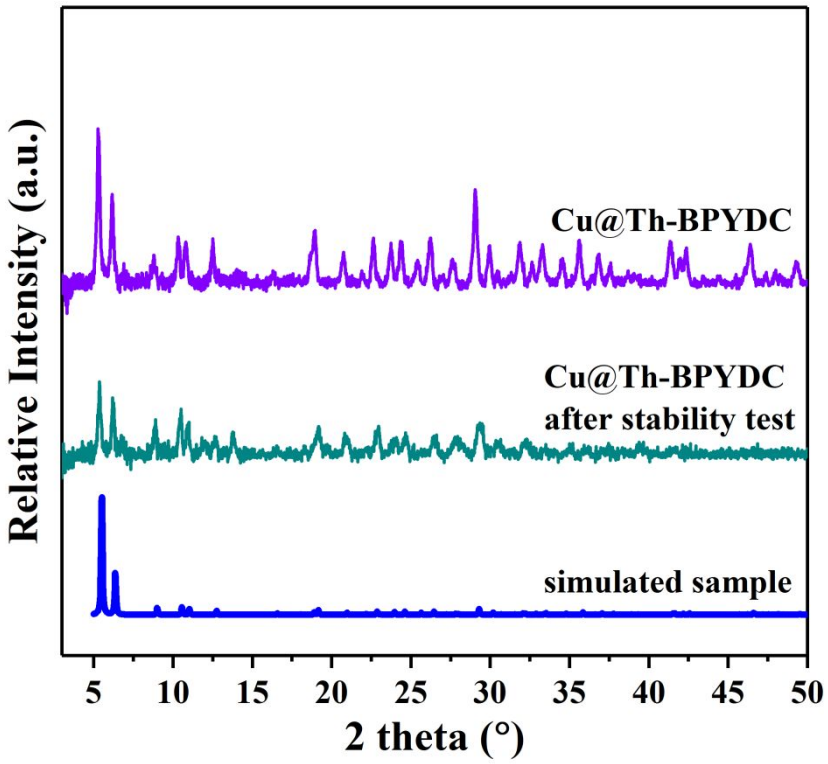

Figure S8. XRD patterns of Cu@Th-BPYDC before and after 1000 CV cycles.

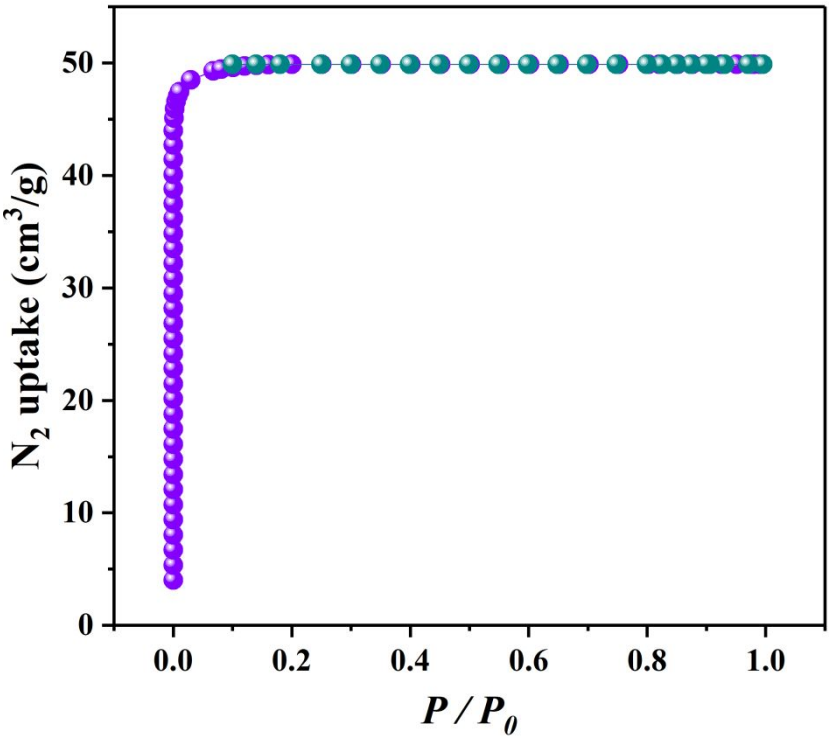

Figure S9. The N_2 adsorption of Cu@Th-BPYDC after stability test for NO_3^- electroreduction at 77 K.

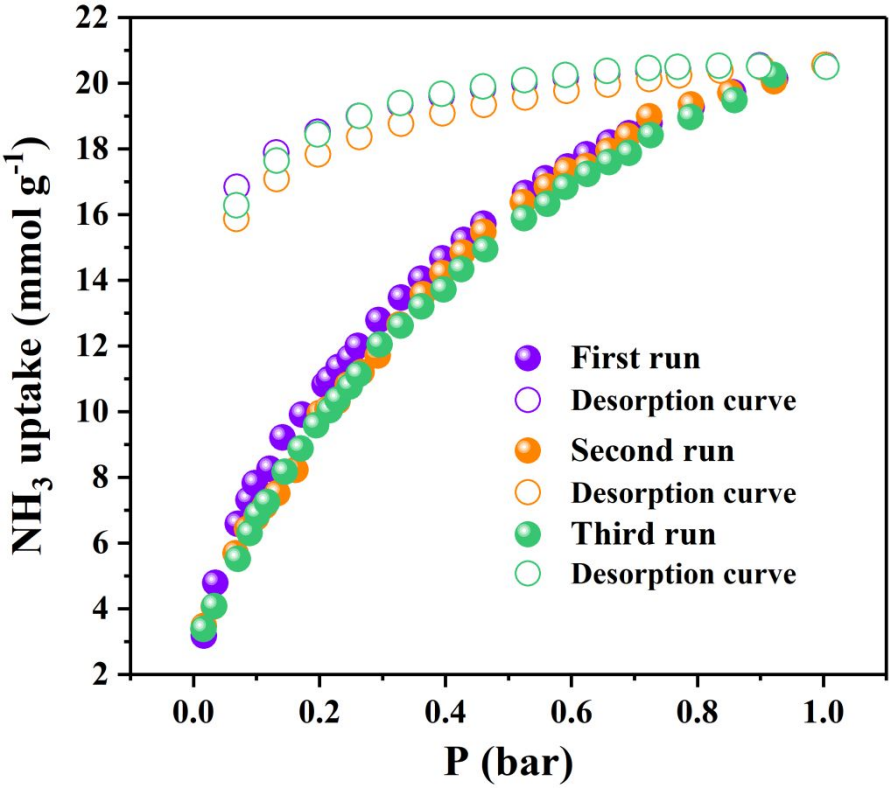

Figure S10. The reusability of Cu@Th-BPYDC toward NH_3 uptake.

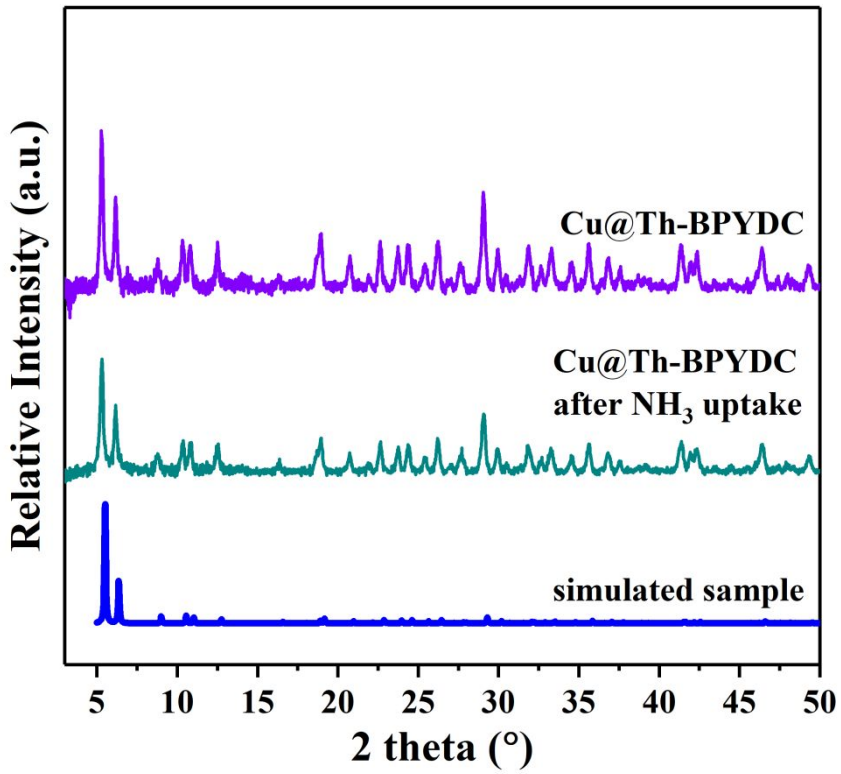

Figure S11. XRD patterns of Cu@Th-BPYDC before and after NH_3 uptake.

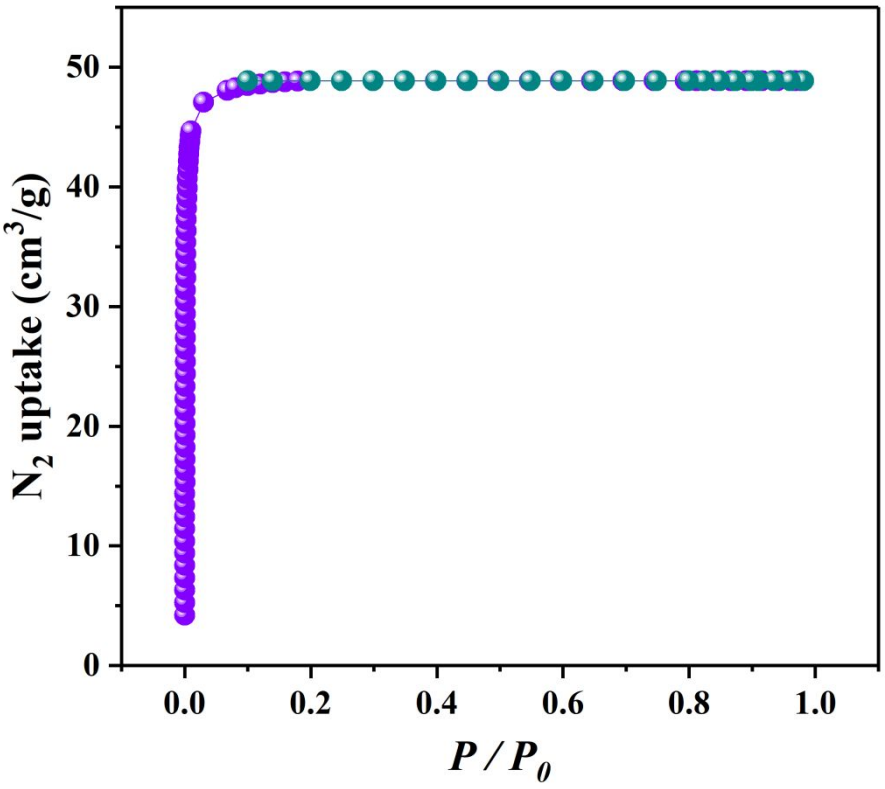

Figure S12. The N_2 adsorption of Cu@Th-BPYDC after NH_3 uptake at 77 K.

Table S1. The comparison of the NH_3 synthesis activity of Cu@Th-BPYDC in NO_3^- electroreduction with other catalysts under ambient conditions.

Catalyst	System	Conditions	NH_3 Yield rate	Faradaic efficiency	Ref.
Cu@Th-BPYDC	1 M KOH + 100 mM KNO_3	Ambient conditions	225.3 μmol h^{-1} cm^{-2}	92.5 %	This work
PTCDA/O-Cu	0.1 M PBS NO_3^- reduction	Ambient conditions	436±85 μg h^{-1} cm^{-2}	77±3%	Nat. Energy 2020, 5, 605–613
Co/CoO NSAs	0.1 M Na_2SO_4, $NaNO_3$	Ambient conditions	194.46 μmol h^{-1} cm^{-2}	93.8 %	Sci. China. Chem. 2020, 63, 1469–1476
B_4C nanosheet	0.1 M HCl	Ambient conditions	0.16 μmol h^{-1} cm^{-2}	15.95 %	Nat. Commun. 2018, 9, 3485
BiNCs	K_2SO4 /H_2SO_4	Ambient conditions	52 μmol h–1 cm-2	66 %	Nat. Catal. 2019, 2, 448-456
Au6/Ni Nanoparticles	0.05 M H_2SO_4	Ambient conditions	0.87 μmol h^{-1} cm^{-2}	67.8 %	J. Am. Chem. Soc. 2019, 141, 14976-14980
Mo^0/GDY	0.1 M Na_2SO_4	Ambient conditions	145.4 μg h^{-1} mg_{cat}^{-1}	21 %	J. Am. Chem. Soc. 2019, 141, 10677-10683

Table S2. Static NH_3 capacities of reported MOFs adsorbents at 298 K and 1 bar.

adsorbents	NH_3 capacity (mmol g^{-1})	Ref.
Cu@Th-BPYDC	20.55	This work
Mg_2(dobpdc)	23.90	Angew. Chem. Int. Ed. 2020, 132, 22720-22725
Cu_2Cl_2BBTA	19.79	J. Am. Chem. Soc. 2018, 140, 3461-3466.
Co_2Cl_2BBTA	17.95	J. Am. Chem. Soc. 2018, 140, 3461-3466.
3D-[Zn_2(L1)$_2$(bpe)]	17.8	ACS Appl. Mater. Interfaces 2017, 9, 37419- 37434.
Fe-MIL-101-SO_3H	17.80	Chem. Sci. 2017, 8, 4399-4409
Mg-MOF-74	~16.2	Chem. Eur. J. 2014, 20, 15611-15617.
P1-PO_3H_2	18.7	Chem. Sci. 2017, 8, 4399-4409.
COF-10	15	Nat. Chem. 2010, 2, 235-238.
[SrOOC]$_{17}$-COF	14.30	ACS Cent. Sci. 2018, 4, 748-754.

References

1. Yanai, T.; Tew, D.; Handy, N. A new hybrid exchange-correlation functional using the Coulomb-attenuating method (CAM-B3LYP). *Chem. Phys. Lett.* **2004,** *393*, 51-57.

2. Becke, A. D. Density-functional thermochemistry. III. The role of exact exchange. *J. Chem. Phys.* **1993,** *98*, 5648-5652.

3. Miehlich, B.; Savin, A.; Stoll, H.; Preuss, H. Results obtained with the correlation-energy density functionals of Becke and Lee, Yang and Parr. *Chem. Phys. Lett.* **1989,** *157*, 200-206.

4. Less, C.; Yang, W.; Parr, R. G. Development of the Colle-Salvetti correlation-energy formula into a functional fo the electron density. *Phys. Rev. B* **1988,** *37*, 785-789.

5. Frisch, M. J.; Trucks, G. W.; Schlegel, H. B.; Scuseria, G. E.; Robb, M. A.; Cheeseman, J. R.; Zakrzewski, V. G.; Montgomery, J. A.; Stratmann, J. R. E.; Burant, J. C.; Dapprich, S.; Millam, J. M.; Daniels, A. D.; Kudin, K. N.; Strain, M. C.; Farkas, O.; Tomasi, J.; Barone, V.; Cossi, M.; Cammi, R.; Mennucci, B.; Pomelli, C.; Adamo, C.; Clifford, S.; Ochterski, J.; Petersson, G. A.; Ayala, P. Y.; Cui, Q.; Morokuma, K.; Salvador, P.; Dannenberg, J. J.; Malick, D. K.; Rabuck, A. D.; Raghavachari, K.; Ortiz, J. V.; Baboul, A. G.; Stefanov, B. B.; Liu, G.; Liashenko, A.; Piskorz, P.; Komaromi, I.; Gomperts, R.; Martin, R. L.; Fox, D. J.; Keith, T.; Al-Laham, M. A.; Peng, C. Y.; Nanayakkara, A.; Challacombe, M.; Gill, P. M. W.; Johnson, B.; Chen, W.; Wong, M. W.; Andres, J. L.; Gonzalez, C.; Head-Gordon, M.; Replogle, E. S.; Pople, J. A. *Gaussian 16*, A. 03; Gaussian, Inc.: Wallingford, CT, 2016.

6. Schuchardt, K. L.; Didier, B. T.; Elsethagen, T.; Sun, L.; Gurumoorthi, V.; Chase, J., Li, J.; Windus, T. L. Basis Set Exchange: A Community Database for Computational Sciences. *J. Chem. Inf. Model.* **2007,** *47*, 1045-1052.

7. Feller, D., J. The Role of Databases in Support of Computational Chemistry Calculations. *J. Comp. Chem.* **1996,** *17*, 1571-1586.